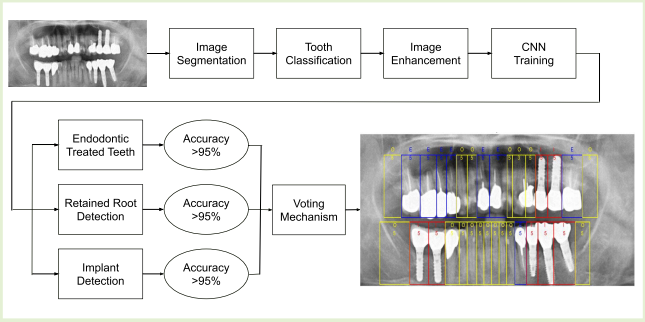
Automated Detection System Based on Convolution Neural Networks for Retained Root, Endodontic Treated Teeth, and Implant Recognition on Dental Panoramic Images

Shih-Lun Chen, *Member, IEEE*, Tsung-Yi Chen, Yi-Cheng Mao, Szu-Yin Lin, *Member, IEEE*, Ya-Yun Huang, Chiung-An Chen, Yuan-Jin Lin, Yo-Ming Hsu, Chi-An Li, Wei-Yuan Chiang, Kai-Yi Wong, and Patricia Angela R. Abu, *Member, IEEE*

***Abstract*—For a daily dental practice, the Panoramic (PANO) X-ray film is one of the most commonly used dental X-rays. One of its important advantages is the coverage of most anatomic structures and clinical findings in a single film. Important information about clinical treatment and diagnosis can be provided from the expert analysis of the PANO. Combined with the assistance of artificial intelligence, the application has great potential. The purpose of this study was to propose an automated detection system based on several modern convolutional neural networks (CNNs) for the classification of retained roots, endodontic treated teeth, and implants. In order to meet the standards of practical clinical application, the database used in this study is provided by dentists with more than three years of practical experience. The contributions of this work are given as follows: 1) proposed more advanced techniques for image segmentation and image position in dental radiographs; 2) a better image enhancement is proposed, which improves the accuracy of the five CNNs to more than 96%; and 3) combined with the fuzzy operation to achieve more powerful and accurate anomaly detection. The final result has an accuracy rate of up to 98.75%. It is about 20% higher than previous techniques. This research designed to identify and document each specific finding automatically could help dentists obtain an objective treatment evaluation and provide dentists more precious clinical time for dental operations and communication with patients.**



***Index Terms*— Convolutional neural network (CNN), image enhancement, image segmentation, Panoramic (PANO), tooth disease recognition.**

I. Introduction

With the development of science in the past two decades, cross-disciplinary research derived from precision medicine has become more and more popular. The research and design personnel collaborates with physicians in various disciplines to study a large amount of patient data through comprehensive application and to carry out the combined application of many innovative technologies. The deep learning technique makes significant advances in medicine by processing patient data and data from comprehensive studies around the world, such as X-ray angiography [1], computed tomography (CT) [2], gastroscopy [3], and other imaging-related medical programs. It is also significantly helpful for the diagnosis of medical imaging symptoms, such as pneumonia detection [4], virus detection [5], tumor lesions [6], and vascular analysis [6].

Manuscript received 5 August 2022; revised 19 September 2022; accepted 22 September 2022. Date of publication 10 October 2022; date of current version 30 November 2022. This work was supported in part by the Ministry of Science and Technology, Taiwan, under Grant MOST-111-2813-C-033-012-E, Grant 111-2813-C-033-013-E, Grant 111-2221-E-033-041, Grant 111-2823-8-033-001, Grant 111-2622-E-131-001, Grant 110-2223-8-033-002, Grant 110-2221-E-027-044-MY3, Grant 110-2218-E-035-007, Grant 110-2622-E-131-002, Grant 109-2622-E-131-001-CC3, Grant 109-2221-E-131-025, and Grant 109-2410-H-197-002-MY3; and in part by the National Chip Implementation Center, Taiwan. The associate editor coordinating the review of this article and approving it for publication was Dr. Brajesh Kumar Kaushik. *(Corresponding author: Szu-Yin Lin.)*

This work involved human subjects or animals in its research. Approval of all ethical and experimental procedures and protocols was granted by the Research Institution Review Board (IRB) under Application No. 202002030B0.

Please see the Acknowledgment section of this article for the author affiliations.

Digital Object Identifier 10.1109/JSEN.2022.3211981

1558-1748 © 2022 IEEE. Personal use is permitted, but republication/redistribution requires IEEE permission.
See https://www.ieee.org/publications/rights/index.html for more information.

Authorized licensed use limited to: Chung Yuan Christian University. Downloaded on December 15,2022 at 06:18:49 UTC from IEEE Xplore. Restrictions apply.

The Panoramic (PANO) X-ray film is one of the most commonly used dental radiographic examinations in daily dental practice. It has many advantages, including good patient acceptance, ease of use, short time of the operating procedure, and, most importantly, coverage of most anatomic structures and clinical findings in a single film [8]. In other words, it shows the visualization of the lower jaw and adjacent anatomical structures, which includes the teeth, upper jaw, lower jaw, surrounding structures, and tissues [9]. Unlike other dental PANO film findings, retained dental root and endodontic treated teeth are highly recognizable in the PANO film. Further invasive treatment procedures are relatively risky to the patient. If symptoms can be detected early, corresponding policies can be proposed. However, owing to the fact that a single PANO film contains a large amount of radiographic information, identifying and documenting each specific finding are often time-consuming and tedious, wasting precious clinical time. Healthcare professionals have only been able to examine dental panoramic radiograph (DPR) manually in the past few decades. With the aid of artificial intelligence, identifying and documenting each specific finding automatically could help save dentists more precious clinical time for communication with patients and dental operations [10]. This study aims to implement a system that classifies diseased teeth from the PANO through convolutional neural networks (CNNs). The prevalence of retained roots was the most common finding in radiological examinations. The prevalence varies from study to study where approximately 15.4%–37.3% of edentulous patients have at least one retained root [11]. Root canal therapy (RCT) is a common treatment that a dentist performs to protect a tooth. Surgery is performed to save severely damaged teeth and repair infected teeth [12]. Osteogenesis of implants is a dynamic process. A prerequisite for the success of the implant is considered to be stable. Especially for implants in bone, an important factor for their long-term success is its early healing stage [13]. Therefore, it is important to fast-track the changes in implants. However, the image-recognizing process is a series of processes that simplify the information given by the image. Normally, people adjust the color and the brightness of the image to differentiate the target. However, the PANO radiograph is a difficult case to find the target since the contrast of the teeth is less protruding than its background. Also, the dark areas that are supposed to be black in color no longer appear to be black due to reflections. The DPR has an image distortion problem. It may cause a loss of detail. In view of this, a Gaussian high-pass filter is used to sharpen images for correction in [12]. It improves image quality and intensifies edges to differentiate between teeth and mouths. In [15], histogram equalization is widely used in image enhancement methods. It adapts the lower contrast areas to a higher contrast by diffusing the most common pixel intensity values and stretching the intensity range of the image to achieve enhancement of subtle areas.

Nowadays, the number of patents that utilize machine learning and big data analysis to identify or classify objects has progressively increased, for example, using machine learning in an indoor location fingerprint positioning. Comparing four different algorithms to find the best result combination is done in [16]. In the examination, a model of hybrid deep learning and machine learning is proposed to classify normal from anomalous ones in proposed in [17]. It focuses on the detection of caries or periapical infections. It shows that applying contrast enhancement while extracting features can achieve higher efficiency and accuracy in the output. Image processing was considered a necessary procedure. In this study, training a CNN model requires a large number of clinical images. Each image contains a tooth and the number of images of the diseased tooth. In the past study in [18], it is proven that the CNN models are suitable for solving the tooth numbering and condition recognition problem of DPR images. Moreover, it can be found that image preprocessing and image augmentation methods are useful. To meet the requirement for the number of clinical images for training, a simple method is proposed in [19]. Flipping images using horizontal and vertical flipping techniques or rotating images at different angles are performed to increase the database required for training. This technique is only used in the training database and will not affect the validation part. This study compares the accuracy of classifying lesion teeth of DPR between five CNN models, including GoogLeNet (InceptionNet), AlexNet, VGG19, ResNet50, and Resnet101. Each model contains different amounts of layers and nodes. To improve the accuracy of the final result, a majority voting scheme based on the histogram within the detected target in the PANO image was proposed in [20]. It is well known that fuzzy decision-making aids achieve excellence in many research fields, for example, power control [21] and forecasting [22]. In [23], a new type of fuzzy decision is implemented under the basic rules of machine language. In this study, a fuzzy decision is proposed to be added in order to perform the intersection operation of the output results of the five models, therefore producing a different classification methodology. The novelties of the proposed method in this study are given as follows.

1) The proposed method uses the concept of the Reimann sum to separate the jaws. This implies that the more pieces the image was segmented, the more the curve will be close to the actual curvature of the jaws.
2) The Gaussian high-pass filter is used to extract the lesion portion of the tooth to enhance the edge, which can guarantee the integrity of the targeted tooth.
3) Generate the accumulated pixel value-line chart of each column of the upper jaw and the lower jaw. After that, the local minimum of the line chart is determined by the slit. This method is used in this study since the jaw separation process outputs two images: the upper jaw and the lower jaw. This makes the slit capture method easier and faster to execute.
4) Combined with the fuzzy operation, the reliability of the final result can be improved.
5) From the results, the accuracy rates of the five models are all above 96%. Among them, the accuracy rate of GoogLeNet reached 98.20%. Compared with the previous literature, the accuracy rate is improved by about 20%.

The proposed method has the capability to fit different curvatures of the jaws. Even if the right-hand side is not

Authorized licensed use limited to: Chung Yuan Christian University. Downloaded on December 15,2022 at 06:18:49 UTC from IEEE Xplore. Restrictions apply.

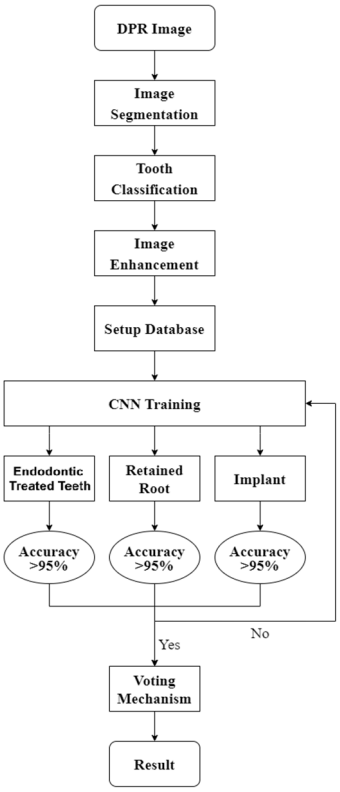


Fig. 1. Flowchart of the system used in this study.

symmetric to the left side, it still reached an average accuracy of 98.2%. Among them, the accuracy of a single illness is over 99%. By using five different models, it allows the construction of a voting mechanism, thus providing a more reliable result.

II. Methodology of the Proposed Solution

In this study, image segmentation and enhancement will be the most important parts that affect the training results of CNN models. In the automatic tooth segmentation stage, the main focus is on segmenting and cropping out the image of a single tooth as the main goal. Because a clinical image of a single tooth is not disturbed by bilateral teeth, it would be the best dataset image for CNN training and judgment. Image enhancement was used to highlight the features of suspected lesions in each tooth. This yields better results when training the model with CNN. The overall flowchart of the study is presented in Fig. 1.

The study in [8] proposed a segmenting algorithm by utilizing the neckline to find the floss line, which is used to separate the jaws and also find the slit by reusing the same curve. This way it allows segmenting each tooth faster and more efficiently. On the other hand, in order to bring the movement curve closer to the mandible (or maxilla), it calculates the magnitude and angle of the directional gradient. Then, it uses the tooth edge slope in the original image and combines it with the masking technique to enable a better clinical image. However, the algorithm requires manual intervention to locate the front teeth and determine the missing tooth in some cases, which leads to inefficiencies when applied in practice.

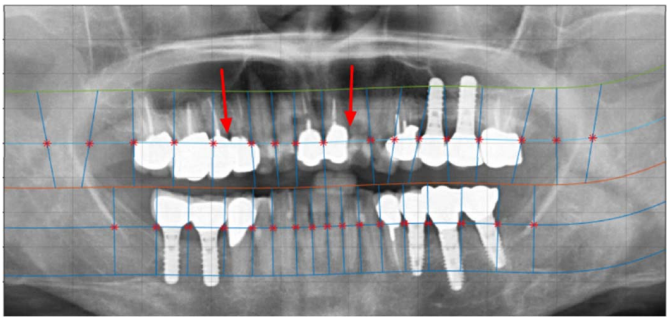


Fig. 2. Using the [8] method of image segmentation will cause a crop to be missed.

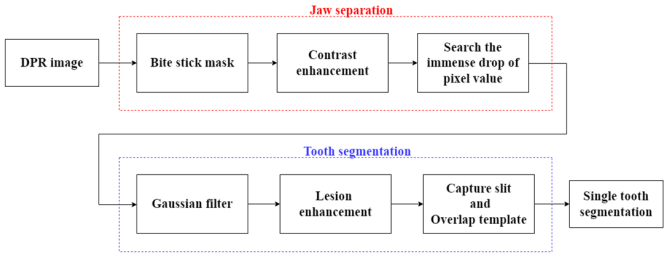


Fig. 3. Process chart for the image segmentation.

As a matter of fact, capturing the slit by finding the local minimum of the whole image has been performed in [8]. It is possible that finding the local minima is affected by the brightness of the implant. The valleys of the accumulated sun of pixel values near some specific treatments may disappear, as shown in Fig. 2. In this article, adjustments were proposed to address this issue. The template divides the image into several blocks. It makes every slit appear and finds each local minimum according to the region. In this way, even if the region template with the high pixel value is processed, the slit can still be found. The detailed steps are described in Section II-A.

A. Image Segmentation

The original image of DPR performs the complete anatomic structures of the lower part of the face, which contains the nonpriority part, such as the cheekbone. Since this research focuses only on the teeth part, in this section, the initial aim is to extract the tooth part from the original DPR image. Generally, a human adult has 32 teeth, including the four third molars. In order not to miss any tooth, the segmentation process will produce 32 images only containing a single tooth in each of them [24]. The process can be separated into two parts: jaw separation and tooth segmentation. First, the upper jaw is separated from the lower jaw, and then, the tooth segmentation process is performed. This will produce a more specific output image than directly utilizing the tooth segmentation process only. Fig. 3 shows the process chart of the segmentation process. Due to the fact that more interference remains, the possibility of misjudging will rise. Thus, the very first process is to capture the oral part of DPR. A rough bounding square that contains only the oral part is obtained by stating the images in the database.

Authorized licensed use limited to: Chung Yuan Christian University. Downloaded on December 15,2022 at 06:18:49 UTC from IEEE Xplore. Restrictions apply.

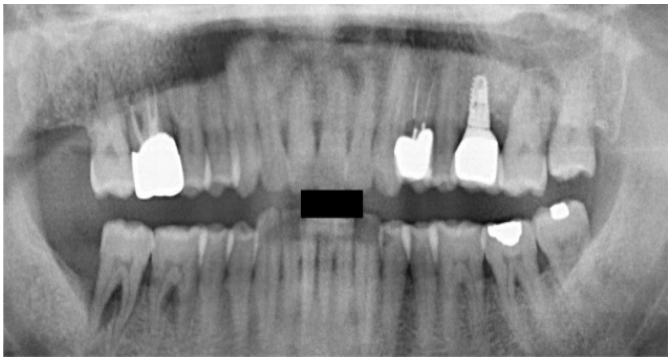


Fig. 4. Schematic of masking the area of the bite stick.

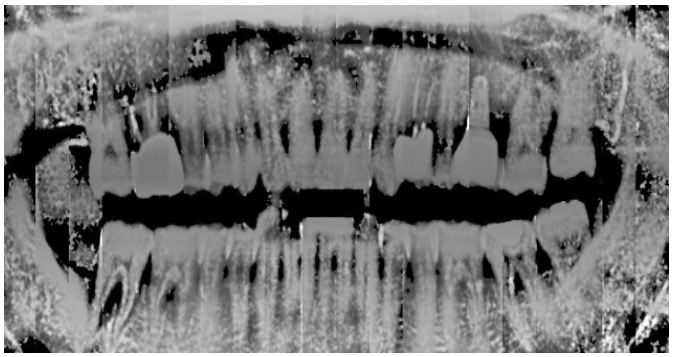


Fig. 5. Image after the morphological operation.

1) Jaw Separation: In this study, image processing was implemented due to the very similar pixel values between the foreground and the background. The first step is capturing the teeth of the PANO by the upper jaw and the lower jaw. Then, image preprocessing is used to highlight the foreground parts to avoid the teeth being disturbed by the background during later cropping. However, the brightness difference between the lower and upper rows of teeth in the PANO causes the image preprocessing to fail to produce the best cropping points. Therefore, the upper and lower rows of teeth must be segmented before image preprocessing.

The accurate region between jaws is relatively darker than the teeth in radiographs. Therefore, restricting the coordinates of cropping in a fixed value might obtain useless parts that directly affect the results of tooth segmentation. Instead of using the fixed coordinate, the concept of the Riemann sum is used. It divides the image vertically into N blocks. Then, it takes $f(t_i)$ as the actual curve, and calculate the vertical midpoint of the arc gap by multiplying $f(t_i)$ by Δx in each block to approximate the actual curve. The Riemann sum formula [25] is shown in the following equation:

$$\sum_{i=0}^{n-1} f\left(t_i\right)\left(x_{i+1}-x_i\right). \tag{1}$$

a) Bite stick mask: It is necessary to let patients nibble the bite stick while taking the PANO radiograph. However, the brightness of the bite stick is similar to the brightness of the teeth in the PANO radiograph, thus making it a challenge to find the pixel valleys near the front teeth. Overlaying a mask of the same size as the bite stick can achieve discontinuity among the upper front teeth and the lower front teeth, as shown in Fig. 4.

Mathematical morphology is a technique for analyzing and manipulating geometric structures, which is a popular tool that is widely used in image processing. One of the most important methods in mathematical morphology is the top-hat transform [26]. The top-hat transform is used to extract the features of the image based on dilation and erosion.

In morphology, two basic operations that are erosion and dilation are applied to either binary images or gray scale. Dilation is an operation that adds pixels to the edge of the object making its boundaries larger. Erosion would remove pixels from the boundaries. Let $A(x,\ y)$ represent a gray-scale image. The process can be achieved by utilizing the structural elements $B(i,\ j)$ following (2) and (3)

$$A \oplus B = \max\left(A\left(x-i, y-j\right)+B\left(i, j\right)\right) \tag{2}$$

$$A \ominus B = \max\left(A\left(x-i, y-j\right)-B\left(i, j\right)\right). \tag{3}$$

The white top-hat transform (WTH) and the black top-hat transform (BTH) are the two categories in the top-hat transform [26]. WTH extracts pixels that are brighter than its surrounding. On the contrary, BTH extracts pixels that are darker than its surrounding. The operation is defined using the following equations:

$$\mathrm{WTH}\left(x, y\right) = A\left(x, y\right) A\left(x, y\right) \circ B \tag{4}$$

$$\mathrm{BTH}(x, y) = A(x, y) \bullet A(x, y). \tag{5}$$

b) Immense drop of pixel value: The resulting image of the morphological operation is shown in Fig. 5. It shows a large drop in pixel values between the crown and the jaws. In this case, the jaw separation process will be easier. As mentioned above, the separation process will utilize the concept of the Riemann sum. First, the image is divided into several pieces. For each piece, the difference in brightness between pixels in pairs from column 350 to column 500 in the sequence is compared. This approximates the area where there is a gap and defines the point where the value drops significantly and rises as Pupper the Plower, respectively. The segment coordinate is considered the midpoint of the Pupper and Plower. For the upper jaw, the part below the segment point is removed. As for the lower jaw, the part below the segment point should remain. The last step is to combine the images side by side, and then, the jaw separation is done.

2) Tooth Segmentation: The ultimate goal of this research is to use CNN models to identify diseased teeth in X-ray films. Therefore, the judgment and extraction of a single tooth at this stage will be the primary goal. In general, the pixel value of the interspace is almost the same as that of the jaw space, which is an ideal basis for separating the teeth. However, the arrangement of the teeth is not a simple task as expected. Other symptoms can increase the difficulty of extracting DPR images, including the impaction tooth or the missing tooth. This makes the segmentation process a crucial task. In order to precisely locate the boundaries of each tooth, this study used two methods: capturing slits and overlapping templates.

Authorized licensed use limited to: Chung Yuan Christian University. Downloaded on December 15,2022 at 06:18:49 UTC from IEEE Xplore. Restrictions apply.

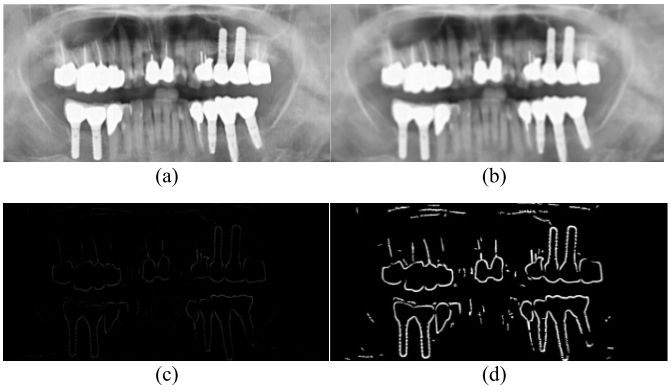


Fig. 6. Actual results of each part of the Gaussian filter. (a) Original image; (b) after the process of Gaussian low-pass filter; (c) subtracting (b) from (a); and (d) enhancing the linewidth of (c).

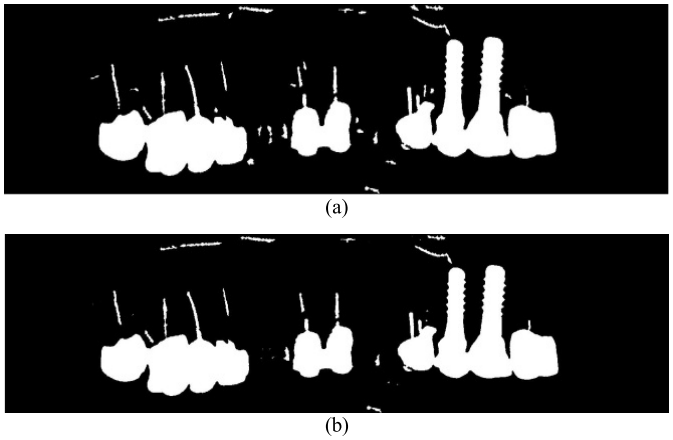


Fig. 7. Extract ROI by binarization with adapting threshold: (a) before covering the small area and (b) after covering the small area.

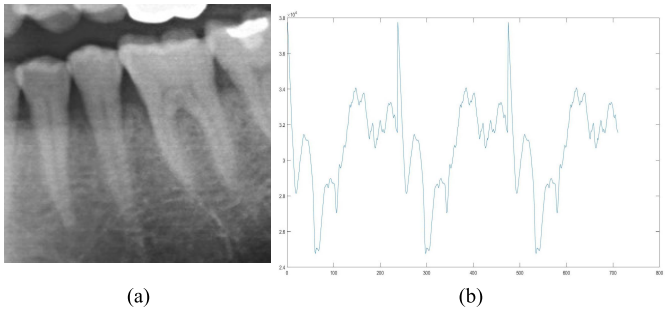


Fig. 8. Sum of pixel value at the slit will present a valley in the line chart. (a) Slit and (b) accumulated pixel value line chart of (a).

a) Gaussian filter: The Gaussian low-pass filter is widely used in image processing since the Gaussian distribution is characterized by a very similar probability distribution of discrete random variables. It has a very good effect in blurring images or removing noise and making the details more evident. It is similar to the averaging filter, but the weight values are not as flat as the average filter. The Gaussian low-pass filter outputs a smoother and less noisy image, i.e., the edges of objects in the image are removed during processing.

Equation (6) presents the Gaussian function [27], where σ is the standard deviation and x is the gray value of each pixel

$$G(x) = \frac{1}{\sqrt{2\pi\, e^2}} e^{-\frac{x^2}{2\sigma^2}}. \tag{6}$$

Subtracting the resulting image of the Gaussian low-pass filter from the original image will obtain the edge image, as shown in Fig. 6.

b) Lesion enhancement: The pixel value of the implant tooth and endodontic treated teeth will have a higher pixel value in DPR, which is an important reference for CNN to distinguish diseased teeth from normal teeth or classify lesions. To emphasize the brighter part, the first step is binarization. The threshold is a value that multiplies the standard deviation of the image σ lesion by 1.75 and adds the average of the entire image M. The function is presented in (7), where $I(x, y)$ represents the input image. If the pixel value at (x, y) is greater than the threshold, the pixel value at that particular coordinate will be set to 255, else 0

$$I(x, y) = \begin{cases} 0, & \text{if } I(x, y) < M + 1.75 \cdot \sigma_{\text{lesion}} \\ 255, & \text{if } I(x, y) \geq M + 1.75 \cdot \sigma_{\text{lesion}}. \end{cases} \tag{7}$$

Using the pixel value to extract the region of interest (ROI) does not only obtain the ROI but also the pixels, which has a higher value than the threshold. Fig. 7(a) shows those that will also be considered noise in the image. Since the image is binarized, the white areas can be simply calculated and covered with a mask if any of which is too small. The results are shown in Fig. 7(b). The lesion enhancement is finished by adding the binarization image to the original image.

c) Capturing slit: As mentioned above, using the characteristic of the slit is an efficient way for locating them by plotting the sum of the vertical pixel value and accumulation of each row. Since the interdental space is usually a darker triangle, it can be judged by the minimum value. This cropping method first calculates the vertical sum of all pictures. Then, the vertical sum from left to right is compared. If it is a trough, the left and right changes are more severe, which can be regarded as a gap between the teeth. Then, the coordinates are recorded as subsequent cutting points. However, unlike the incisors that are perpendicular to the ground, molars are usually oblique. Therefore, when marking the position of the molars, the cutting point is set margin for around 10 pixels on the left and the right. The valley of the line chart will be considered as the position of the slit, as illustrated in Fig. 8. Since there is no slit at the left of the very last tooth on the left jaw, the first reference point for tooth segmentation is set as 100, which approximates the position where the tooth appears.

3) Overlapping the Template: Capturing a slit is a powerful method to separate the teeth. However, the ideal applying situation is the interval, amid each tooth is big enough to detect the descending. In particular cases, such as impacted, missing, or crooked teeth, it will cause difficulty in identifying the slit. To compensate for the failure to capture the slit, an overlay of a template, which is the average width of each tooth, was used to find the approximate location of the border.

Authorized licensed use limited to: Chung Yuan Christian University. Downloaded on December 15,2022 at 06:18:49 UTC from IEEE Xplore. Restrictions apply.

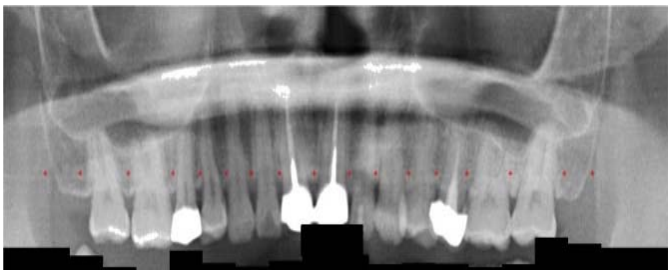


Fig. 9. Overlapping the template on the image where the red points represent the templates.

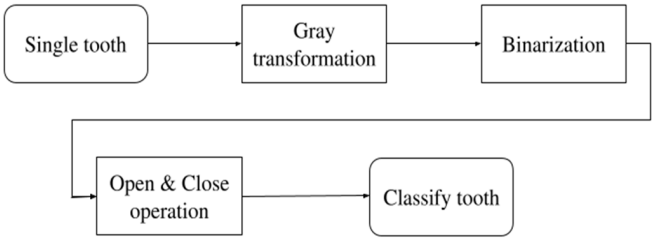


Fig. 10. Image enhancement flowchart was used in this research.

The result of using the template, which consists of statistical data, is too rough; thus, the process of correction is necessary. By taking the left–right symmetry of the mandible, the template can be superimposed on the radiograph locating it. This can be achieved by limiting the drop detection range to the position of the bite bar that is bitten by the anterior teeth. After locating the center of the jaw, the first step is calculating the distance between the first reference point and the central point in the template and the radiograph. The next step is marking the distance of the template as D1 and the radiograph as D2. The template preserves the ratio between each tooth, while D2 displays the actual distance required. Finally, a linear adjustment is used to make D2 the same length as D1. Through the above steps, customizing the template for each radiograph can be obtained. As shown in Fig. 9, the red points represent the template.

4) Segmentation Process: The segmentation process is carried out from the first point of the reference points. The cropping length is considered the distance to the next point. As for the cropping height, 400 pixels were applied in this study. Statistical data were used as well since the goal of the procedure is to separate the tooth from each other. Therefore, localization and symptom judgment will not be performed.

B. Image Enhancement

In order to improve the accuracy of the CNN training results, highlighting the characteristics of individual diseases is one of the most important parts of this research. Moreover, the different diseases would have different ways of enhancement. The preaction of image processing is required to remove the noise on the graph before the training image is put into the CNN models. The steps for symptom enhancement are shown in Fig. 10.

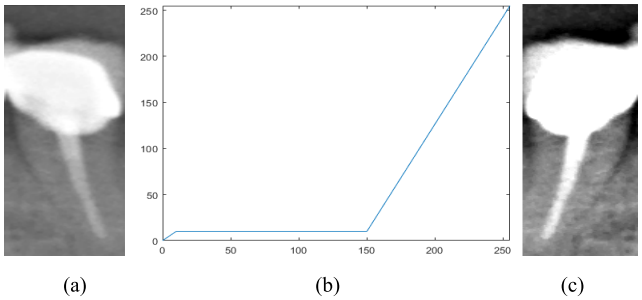


Fig. 11. Process in which endodontic treated teeth undergo linear transformation. (a) Original image. (b) Linear transform model. (c) Transformed image.

1) Gray Level Transformation: Each image of a single tooth could cause different gray-scale contrasts due to different positions and environmental factors after cropping. The gray scale represents the hierarchical level of brightness from darkest to brightest. The more it is in the middle level, the subtler the picture will be. Taking an 8-bit panel as an example, it can represent two out of eight times, that is, 256 levels of brightness, which is called 256 levels of gray scale. Therefore, some cropping images might be concentrated in higher gray-scale areas or in lower gray-scale areas. This makes it impossible for the human eye to directly and clearly identify the difference between the teeth and the background. To highlight the contrast between the background and the teeth and to modify the image pixels, gray-scale transformation is a necessary process in this study.

Gray-scale transformation is one of the important parts of image enhancement. Transforming the gray-scale value of each pixel in the image could expand the dynamic range and contrast of the image. This achieves the goal of having a clear image and with evident features. In this study, different stages and illnesses would take different gray-scale changes.

a) Linear transformation: In order to display the target and the gray-scale regions of interest more clearly, this study adopts a piecewise linear method that can relatively suppress those not of interest areas. For example, Fig. 11 shows the endodontic treated teeth image. In piecewise linear transforms, blocks 0–10 remain unchanged and constant, while blocks from 10 to 150 are constrained to where gray scale equals 10. Blocks from 50 to 255 are distributed according to linear variations from 10 to 255.

b) Histogram equalization: If the peak of the histogram distribution is concentrated somewhere in the middle, the contrast between light and dark is less pronounced. This situation would frequently occur in normal teeth and retained roots. However, the peak would also occur in darker places. Thus, the histogram should be adjusted to brighter places. Taking the endodontic treated teeth as an example, it can be seen with the naked eye that the gray level of the tooth in this image is very close to that of the background, and the gray level of the overall image is lower. It has to be balanced and increase its overall brightness for this image. The change and improvement can be seen in Fig. 12.

2) Binarization: Binarization divides gray-scale images into "black" and "white" by setting a threshold. If the gray-scale

Authorized licensed use limited to: Chung Yuan Christian University. Downloaded on December 15,2022 at 06:18:49 UTC from IEEE Xplore. Restrictions apply.

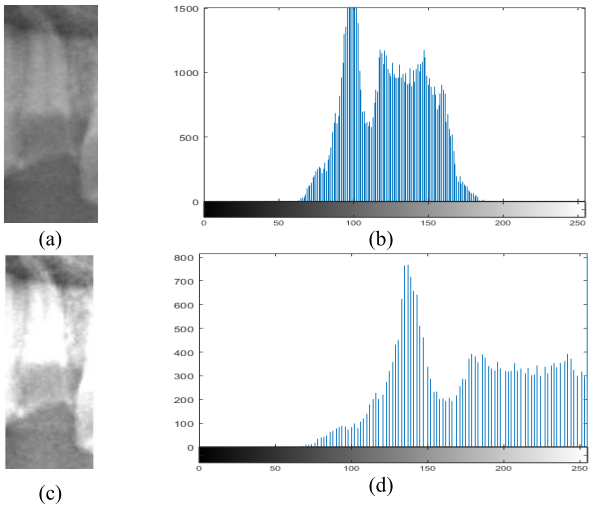


Fig. 12. Histogram equalization for residual. (a) Original image. (b) Original histogram. (c) Equalize image. (d) Equalize histogram.

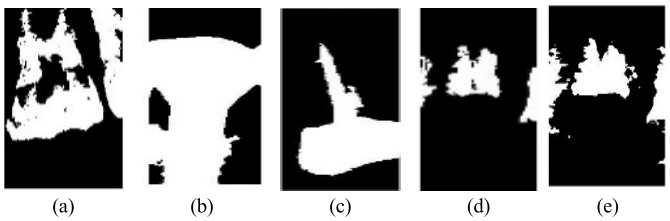


Fig. 13. Results of the clinical image after the binary processing. (a) Normal, (b) implant, (c) root canal, (d) retained root, and (e) retained root after open–close operation.

value is greater than the threshold, it points to the white point. If the gray-scale value is less than the threshold, it points to the black point. This can highlight the outline of the target and effectively reflect the inconspicuous information in the image. In this study, the distribution of histograms was used to set appropriate thresholds for different disease conditions, as shown in Fig. 13.

3) Open–Close Operation: The closed operation is the expansion before erosion. The purpose of the closed operation is to eliminate small objects and smoothen the contours. The open operation is corroded and then expanded. Expansion is a process of expanding the boundaries. First, place them in the background, and then, use a close operation to remove the target. Finally, turn the background into the foreground. Expand the boundary outward. It could be used to fill holes in objects. Corrosion is the process of eliminating boundary points and causing the boundaries to contract internally. It could be used to eliminate small and meaningless objects. The continuous opening and closing operation can significantly increase the area of the object and some misjudgment of holes and background areas scattered with some small noise objects. This study uses the eight-connectivity and three times open–close operation to make images smoother and more favorable to image classification. The formula of the open–close operation [28] is given in the following equations:

$$A \circ B = (A \ominus B)B \tag{8}$$

$$A \bullet B = (AB) \ominus B. \tag{9}$$

C. Image Classification

This method and step would be the last part before setting up the database. In the previous description, image enhancement based on the characteristics of each symptom can classify teeth more effectively at this stage. In this study, the retained root would be prioritized for judgment. The retained root is the tooth that has only part of the obvious disease and no external interference. After image enhancement, bipolar images very similar to normal teeth after binarization are obtained. Thus, the teeth are resized to 200*200 pixels; it would trim the point equal to 100 on the x-axis and the y-axis. The image is divided into four images of equal size: upper left, upper right, lower left, and lower right, and the proportion with black and white in four images is computed. When one of the pieces has more parts of black than the other three pieces over 60%, it could be determined that this image has a high probability to be a retained root. The retained root is a tooth missing a corner of the normal tooth. After properly resizing, the normal tooth would be evenly distributed in the four cropped images, and the retained root had a corner. For example, suppose that the black part of the image in the top left corner has a ratio of 0.782, and the black part in the other three pieces of the image is only up to 0.462 in proportion. In this case, it could be inferred that this single tooth image is likely to be a retained root and automatically imported into the database.

After the identification of the retained root, there are three kinds of teeth remaining: the endodontic treated teeth, the normal teeth, and the implant. They would be classified by using their area, eccentricity, and major axis length without resizing the image. Moreover, a lot of thresholds are set here. The enhanced image is directly used to classify. First, it could be seen that the area of the implant occupies the largest part of the entire enhanced image and has the largest perimeter. It would be the standard to distinguish whether the cropped image is an implant or not. Second, the endodontic treated teeth have one or two endodontics at the root of the tooth. As such, it has the smallest eccentricity in the entire crop image. The last is the normal tooth, which is distinguished after it failed to meet the description of the first two teeth.

D. Disease Recognition Method Using CNN Models

The clinical image database used in this study was collected and annotated by three professional dentists. All specialists have at least three years of clinical experience and are employed in specialized clinics. This research has passed the Research Institution Review Board (IRB) with application number 202002030B0. In addition, the researchers accepted experts to teach symptom knowledge and judge the characteristics of actual cases. The CNN model trained in the research is calibrated according to the clinical data provided by experts to eliminate other nontarget symptoms.

In recent years, many popular CNN-based deep learning models have been introduced, such as AlexNet, GoogLeNet, VGGNet, and ResNet. In this study, we used five popular deep learning models as the representative learning models for disease recognition, including AlexNet, GoogLeNet, VGG19, ResNet50, and ResNet101. In terms of hardware

Authorized licensed use limited to: Chung Yuan Christian University. Downloaded on December 15,2022 at 06:18:49 UTC from IEEE Xplore. Restrictions apply.

TABLE I
HARDWARE AND SOFTWARE PLATFORMS USED IN THIS STUDY

Hardware platform	Version
CPU	AMD R5 3600X
GPU	GeForce RTX 2070 8G
DRAM	DDR4 2666 16G
Software platform	**Version**
MATLAB	R2021a
Deep Learning Toolbox	R2022a
Deep Network Designer	14.2
Layer Library	14.2

performance listed in Table I, this study uses the Nvidia GeForce RTX 2070 GPU to accelerate deep learning CNN model training. In terms of software, this research uses the deep network designer to design the convolutional network model. the pretrained network model for image classification is installed through the Deep Learning Toolbox provided by MATLAB. Besides, the layer library is used to call out the fully connected layer, the softmax layer, and the classification layer. In this study, the parameters of the last three layers in the convolutional neural model proposed are modified through the above layer parameters. Taking AlexNet for example, the original input of AlexNet is set with an image size of 227*227 pixels. In this study, before the model learns, the input image size needs to be reset to 224*224, which is considered to be 224*224*3 (RGB has three channels) in the model. Its neuronal conversion formula is shown in the following equation:

$$y = x \cdot w + b \tag{10}$$

where the output is y, the input is x, the weight is w, and the bias is b.

To avoid training results that are also linear functions, a nonlinear activate function, such as a rectified linear unit (ReLu) layer, is added to remove results less than 0. It also prevents the model from overfitting. There are dropout layers and pooling layers that prevented overfitting in the AlexNet layer. The ReLu activate function formula is shown in the following equation:

$$y = \text{relu}\,(x \cdot w + b)\,. \tag{11}$$

Although there would be a degree of character disappeared, it would not unduly affect the final accuracy. In addition, some of the input images are RGB images, while some are gray-scale images. In order to ensure the same format of the input, the RGB images are modified to gray-scale images to reduce the time spent in model training. In the output layer, AlexNet originally has 1000 types of output images. This study needs to classify four different symptoms only. Therefore, the full connection layer of the third from the last layer in the whole model must be replaced with the output of the four images, the weight of the learning factor is adjusted to 10, the bias of the learning factor is 10, and then, reconnect the softmax layer and the classification layer. Through the deep network designer

TABLE II
NETWORK ARCHITECTURE OF THE ALEXNET

Type	Filters numbers	Activation
Input		224x224x1
Convolution _1	96	54x54x96
Relu_1		54x54x96
Normalization_1		54x54x96
Max Pooling_1		26x26x96
Convolution_2	256	26x26x256
Relu _2		26x26x256
Normalization_2		26x26x256
Max Pooling_2		12x12x256
Convolution_3	384	12x12x384
Relu _3		12x12x384
Convolution_4	384	12x12x384
Relu _4		12x12x384
Convolution_5	256	12x12x256
Relu _5		12x12x256
Max Pooling _5		6x6x256
Fully Connected_1		1x1x4096
Relu _6		1x1x4096
Dropout_6		1x1x4096
Fully Connected _7		1x1x4096
Relu _7		1x1x4096
Dropout _7		1x1x4096
Fully Connected _8		1x1x4
Soft Max		1x1x4
Classification		1x1x4

provided by MATLAB, MATLAB's established CNN model was introduced. Make parameter adjustments, and after the correction is complete, export to the workspace. The individual layers of the AlexNet model used in this study are shown in Table II.

In the augmented data section, the pixel range is adjusted to [−20 20], which is used to pan 20 pixels left and right or up and down during training. It randomly mirrors the image horizontally and vertically to add image data and prevent the model from overfitting. Moreover, in the course of training, there are three major factors that affect learning outcomes. To find the best results in this study, the analysis was carried out through the SGD gradient descent method. This method that calculates the minimum value of the loss function uses the principle of an iterative algorithm. Table III shows the hyperparameters related to the training model in this study. The higher accuracy is obtained by updating the model and the adjustment of the learning rate. Moreover, they have a great impact on the calculation results.

1) Learning Rate: In general, the learning rate must be larger if you want the neural network to learn faster. However, when

Authorized licensed use limited to: Chung Yuan Christian University. Downloaded on December 15,2022 at 06:18:49 UTC from IEEE Xplore. Restrictions apply.

TABLE III
HYPERPARAMETER VALUES USED IN THE PROPOSED ALGORITHM

Initial Learning Rate	0.0001
MaxEpoch	12
Batchsize	16
Learning Rate Drop Factor	0.02
ValidationFrequency	10
LearnRateDropPeriod	3
LearnRateDropFactor	0.02
Shuffle	every-epoch

its learning rate exceeds an extreme value, it causes the loss to stop and oscillate. The smaller the learning rate, the slower the descent along the loss gradient, which also means that it takes more time to converge. When the learning rate is larger, the learning speed of the neural network is faster. However, when it goes beyond the extreme value, the loss stops, and it falls and shakes repeatedly at a certain location. This could lead to bad results. Therefore, the choice of learning rate would be an important part of this topic design. This article uses 0.0001 as the weight of the learning rate. Also, after three epochs, it would reduce the learning rate of the model to 0.02 to speed up the convergence and reduce convergence time.

2) MaxEpoch: An epoch is the time taken to train the entire set of images. However, it is not enough to pass a complete set of data in a neural network at once. It is necessary to transfer multiple times in the same neural network. Too few epochs could not get enough convergence, and too many epochs would lengthen the training time, which might also cause overfitting. Therefore, how many epochs are used to train models is worth thinking about in this study. Several numbers of epochs have been tried in this study: 6, 9, 12, 15, and 18 epochs, where 12 epochs showed the best results among all.

3) Batchsize: The batch is a parameter that used a small sample in the training dataset to reverse-propagate the model. The small sample size is known as "batchsize." There were only about 100 images between the implant and the retained root obtained after image segmentation.

However, this is insufficient for training CNN. Therefore, the single images obtained from each symptom are randomly classified in a 7:3 manner. Among them, 70% are used as the training database, and 30% are used as the verification database. Thus, for 70% of the training database, image flipping and vertical or horizontal translation are used to increase the database data. Furthermore, 350 other teeth are randomly selected as training images, having 1400 total images or 350 pictures per database. The total number of clinical images used in this study is 1400 images and 350 images per disease, as listed in Table IV.

III. EXPERIMENTAL RESULTS

The results of the disease feature enhancement technique proposed in this study are shown in Fig. 14(b). Experimental results show that the proposed method helps to improve the accuracy of CNN training results compared to the original image Fig. 14(a). The comparison of before and after image enhancement is shown in Table V.

TABLE IV
VARIATION IN THE NUMBER OF CLINICAL IMAGES EXPECTED TO BE TRAINED

	Implant	Endodontic treated teeth	Residual root	Other tooth
Original quantity	124	173	156	2231
Select quantity	350	350	350	350

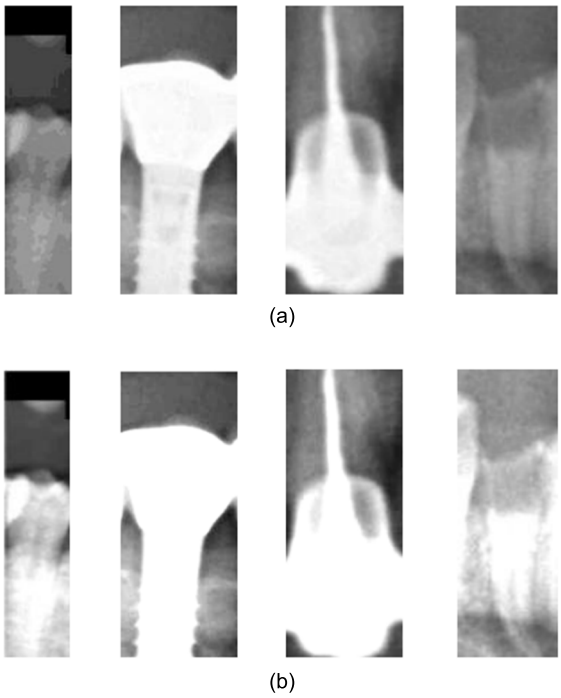


Fig. 14. Results of enhanced processing of clinical image features of each disease. (a) Original image. (b) Enhanced result.

TABLE V
COMPARISON BEFORE AND AFTER IMAGE ENHANCEMENT

	GoogLe Net	AlexNet	VGG19	ResNet 50	ResNet 101
This Work Before Enhancement	93.57%	94.36%	89.48%	92.86%	94.13%
This Work After Enhancement	98.2%	97.13%	96.88%	97.45%	97.38%

TABLE VI
2-D CONFUSION MATRIX IS USED IN THIS RESEARCH

	Real True	Real False
Predict True	Tp (True Positive)	Fp (False Positive)
Predict False	Fn (False Negative)	Fn (True Negative)

To calculate the accuracy of the model, the validation set repository for testing is used and is fed into the trained

Authorized licensed use limited to: Chung Yuan Christian University. Downloaded on December 15,2022 at 06:18:49 UTC from IEEE Xplore. Restrictions apply.

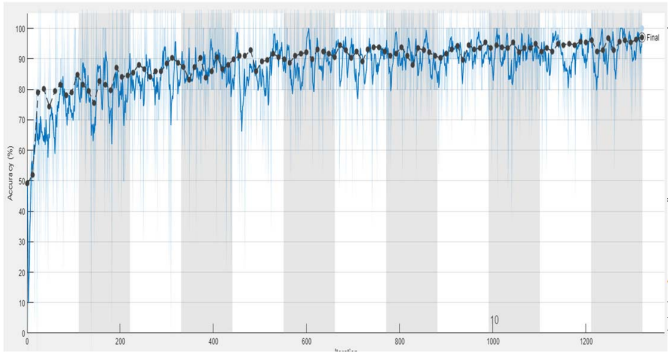


Fig. 15. Accuracy training process of the AlexNet model in the training set (blue line) and the test set (black line).

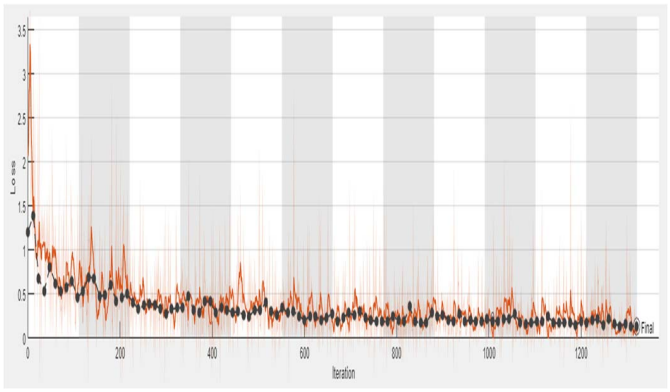


Fig. 16. Loss function with the accuracy of the AlexNet model in the training set (orange line) and the test set (black line) during training.

TABLE VII
COMPARISON BETWEEN LIN'S MODEL AND PROPOSED MODEL

	Method in [17]	This work				
		GoogLe Net	AlexNet	VGG19	ResNet 50	ResNet 101
Accuracy	75.53%	**98.2%**	97.13%	96.88%	97.45%	97.38%
Training time (mm:ss)	03:48	07:25	07:49	28:32	11:18	13:57
Running time(s)	4.81251	4.784189	4.842565	5.732610	4.792792	5.007921

network. The accuracy of the CNN network is calculated based on the actual annotation of the image and the evaluation results of the model. The training process and its accuracy can be obtained from Fig. 15. The loss function during the training process is shown in Fig. 16. For the correct rate algorithm, this study adopts (12) and its calculation methods in Table VI

$$\text{Accuracy} = \frac{\text{Tp} + \text{Tn}}{\text{Tp} + \text{Fp} + \text{Tn} + \text{Fn}}. \tag{12}$$

From the results, the accuracy rates of the five models are all above 96%. Among them, the accuracy rate of GoogLeNet reached as high as 98.20%, as listed in Table VII. This is in contrast to the 75.53% accuracy reported by the study in [17]. According to the accuracy rate of individual diseases, the accuracy rate of the preserved root, endodontic treated teeth, and implant detection technology based on the technology proposed in this article has been successfully increased to more than 94%, and the accuracy has been significantly improved [17], as shown in Table VIII.

TABLE VIII
ACCURACY FOR DIFFERENT DISEASE USE IMPROVE IMAGE

	Method in [17]	GoogLe Net	AlexNet	VGG19	ResNet 50	ResNet 101
Implant	84.30%	99.70%	98.60%	97.70%	98.20%	98.60%
Endodontic treated teeth	76.20%	98.20%	96.70%	99.10%	98.40%	98.40%
Retained root	65.10%	99.60%	98.80%	96.50%	97.10%	98.70%
Others	76.50%	95.30%	94.40%	94.20%	96.10%	93.80%

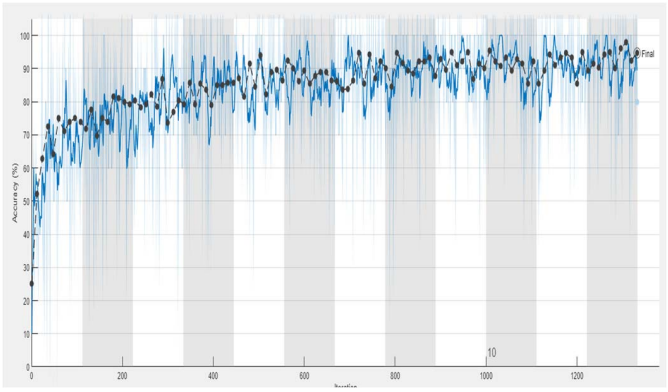


Fig. 17. Accuracy training process using [8] cropping image.

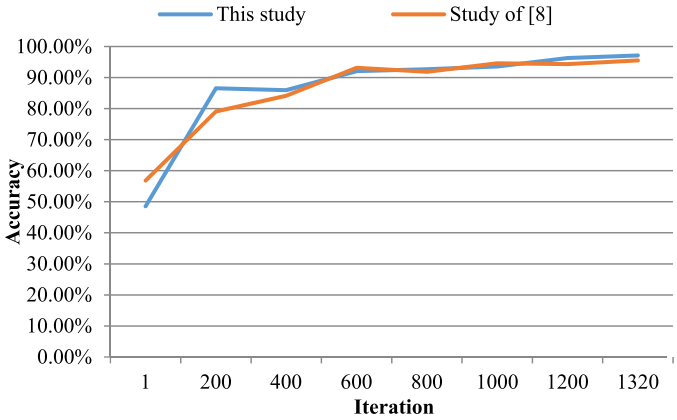


Fig. 18. Comparison of the training process: this study is the blue line, [8] is the orange line, the axis of abscissa is iteration, and the axis of ordinate is accuracy.

The cropping method of [8] to obtain a single tooth image and AlexNet was used in this study for training. Fig. 17 presents the training process of the method of Panetta et al. [8]. Comparing the training process from Fig. 18, it can be found that, even if the cropping method is different, higher accuracy can be obtained. However, using the cropped images of [8] during training cannot achieve effective convergence of the model even if the final accuracy is close to 95%. In contrast, training with cropped images in this study leads to higher accuracy and some degree of convergence accuracy at epoch 12.

Authorized licensed use limited to: Chung Yuan Christian University. Downloaded on December 15,2022 at 06:18:49 UTC from IEEE Xplore. Restrictions apply.

TABLE IX
CLINICAL DATA COMPARE TO THE RESULT

Tooth Position	25	26	27	28
Clinical Data	Implant	Implant	Endodontic	Others
This Work Before Enhancement	95.47% Implant	97.86% Implant	85.39% Endodontic	91.94% Others
This Work After Enhancement	99.28% Implant	99.20% Implant	98.11% Endodontic	98.21% Others

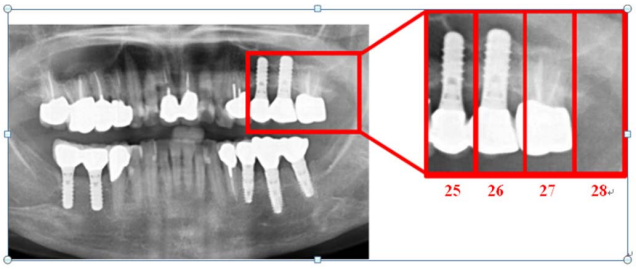


Fig. 19. Outer example for validation using [8] cropping image.

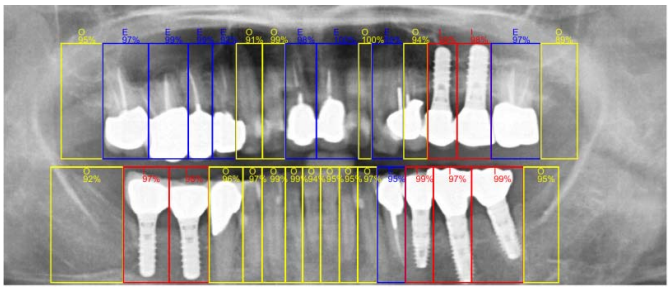


Fig. 20. Result of the framed back to the original image.

Especially in clinical medicine, high-precision judgment is necessary to provide better medical quality. The image recognition capabilities of CNN are excellent enough to fit this need. The practical application of this technique is shown in Fig. 19. The proposed technique is applied to clinical images of patients, and the results are listed in Table IX.

In order to improve the clinical utility and confirm whether the accuracy rate really meets the expectations of this study, the concept of RCNN is introduced. It uses the position of the upper left crop point to select bounding boxes. The length and the width of each bounding box are the size of the cropped image. For example, a DPR image is randomly selected from the database, and then, all teeth are cropped and judged. After which, they are trained with GoogLeNet, and all results are framed back to the original image. From Fig. 20, the teeth judged for each symptom are presented. The accuracy rate is very high, and there are almost no errors. The red frames are the implant, and "I" was used to represent it. The blue frames are the endodontic treated teeth treatments where "E" was used to represent it. The yellow frames are not the target of this study and are called "Other" where "O" was used to represent it. For each box, a corresponding label is placed in the upper part with the disease name and accuracy rate.

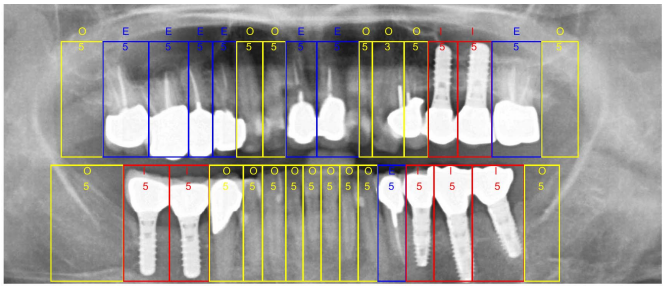


Fig. 21. Final result is displayed using the fuzzy voting system.

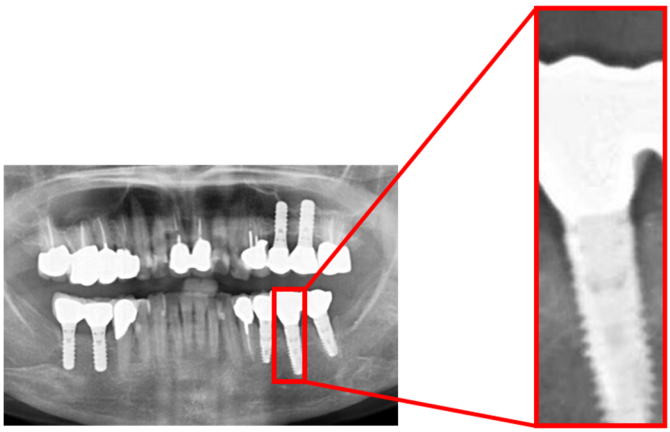


Fig. 22. Outer implant example for validation.

TABLE X
RESULT AFTER JUDGMENT FOR THE SAMPLE IMAGE IN FIG. 22

	Clinical Data	This work					Result of Fuzzy
		GoogLe Net	Alex Net	VGG 19	ResNet 50	ResNet 101	
Accuracy	Implant	97.90% Implant	97.32% Implant	99.10% Implant	99.64% Implant	97.19% Implant	Implant

TABLE XI
SEGMENTING RESULT COMPARING

	Method in [15]	Method in [8]	**This Work**
Accuracy	75.53%	94.64%	**98.75 %**

Furthermore, to minimize the errors, the final result will be judged through a voting mechanism. This study uses five different models to judge outcomes to make fuzzy decisions. If it is determined in the verification that more than three types of outputs are the same, it will give the corresponding result; otherwise, the output will be "Other," as shown in Fig. 21.

The clinical image of a single tooth is illustrated in Fig. 22. Taking this as the target image for judging symptoms, the final actual simulation judgment results of the proposed technology are listed in Table X.

The final experimental results are listed in Table XI, where the accuracy of this work is above 96%. Through the fuzzy voting mechanism, the calculated accuracy reached 99.43%. Comparing this study with [8] and [15], the cropping result

Authorized licensed use limited to: Chung Yuan Christian University. Downloaded on December 15,2022 at 06:18:49 UTC from IEEE Xplore. Restrictions apply.

11	12	13	14	15	16	17	18
5	3+9	3+9	3+9	3+9	4	4	3+9
Others	Root canal	Root canal	Root canal	Root canal	Others	Others	Root canal
21	22	23	24	25	26	27	28
3+9	4	1	3+9	8	8	3+9	5
Root canal	Others	Others	Others	Implant	Implant	Root canal	Others
31	32	33	34	35	36	37	38
5	6	6	6	3+9	4	0	0
Others	Implant	Implant	Implant	Root canal	Others	Others	Others
41	42	43	44	45	46	47	48
0	0	4	4	3	8	8	5
Others	Others	Others	Others	Others	Implant	Implant	Others

Fig. 23. Comparison between the result of the fuzzy voting system and the dentist's judgment.

using [8] reached 94.64%, while model [15] trained using the cropping method in this article achieved 75.53% accuracy.

The results of the voting mechanism were compared with the map provided by the dentist. It was found that most of the teeth were judged as successful. The only special case is the tooth located at position 24 (using the FDI tooth numbering system). The dentist marks the tooth with number 8 as an implant, 9 as the endodontic treated teeth, and another number as "others," as shown in Fig. 23. Number 9 in 24 stands for endodontic treated teeth, but the fuzzy voting system's result is "other." This mistake occurs due to the root of the tooth being skewed. Since the bounding box capture process works better when the root is perpendicular to the horizon, the features of the endodontic treated teeth are eliminated during the segmentation process, leading to false positives. Moreover, in the DPR, 32, 33, and 34 are the implants, but they are marked as "others" in the dentist file. These may be clerical errors when the dentist marks the teeth.

IV. Conclusion

The main goal of this study is to reduce the burden of dentists by automatically detecting three special disease conditions (retained root, endodontic treated teeth, and implant) in the PANO images. The proposed method performs automatic tooth segmentation, cropping, and image enhancement on the periphery of a single tooth. In the trimming step, the technique proposed in this study that separates the jawbone and other regions has been very successful. However, one of the targets identified in this study was the residual root of teeth. If the deep learning solution to separate the jaws and other regions is used directly, there is a higher chance of finding the wrong position. For example, the edge of the mouth can easily be judged as the residual root of teeth. Future work looks forward to adding the use of deep learning for faster processing. It then uses several of the most popular CNN models to train a disease recognition and detection model. In order to ensure that the obtained result is the best solution, fuzzy is used to filter the maximum intersection of five CNN running results. The final result shows an accuracy of up to 98.20%, while its lowest accuracy is at least 96.88%. Even faster R-CNN or YOLO techniques are used to improve the current results at this stage. In the future, this study will continue to classify other kinds of teeth, such as prosthodontics, an implant with suspected bone loss, and impacted teeth with coronal translucence pointing at a cyst identified.

Institutional Review Board Statement

Chang Gung Medical Foundation Institutional Review Board; IRB number: 202002030B0; Date of Approval: 1 December 2020; Protocol Title: A Convolutional Neural Network Approach for Dental Bite-Wing, Panoramic and Periapical Radiographs Classification; Executing Institution: Chang Gung Medical Foundation Taoyuan Chang Gung Memorial Hospital of Taoyuan; Duration of Approval: From 1 December 2020 to 30 November 2021. The Research Institution Review Board (IRB) reviewed and determined that it is expedited review according to case research or cases treated or diagnosed by clinical routines. However, this does not include HIV-positive cases.

Acknowledgment

Shih-Lun Chen, Tsung-Yi Chen, Ya-Yun Huang, and Chi-An Li are with the Department of Electronic Engineering, Chung Yuan Christian University, Taoyuan 32023, Taiwan (e-mail: chrischen@cycu.edu.tw; g10976016@cycu.edu.tw; g11076004@cycu.edu.tw; g10976004@cycu.edu.tw).

Yi-Cheng Mao is with the Department of General Dentistry, Chang Gung Memorial Hospital, Taoyuan 33305, Taiwan (e-mail: louiszzzzz@cgmh.org.tw).

Szu-Yin Lin is with the Department of Computer Science and Information Engineering, National Ilan University, Yilan 26047, Taiwan (e-mail: szuyin@niu.edu.tw).

Chiung-An Chen is with the Department of Electronic Engineering, Ming Chi University of Technology, New Taipei City 24301, Taiwan (e-mail: joannechen@mail.mcut.edu.tw).

Yuan-Jin Lin and Yo-Ming Hsu are with the Department of Electrical Engineering and Computer Science, Chung Yuan Christian University, Taoyuan 32023, Taiwan (e-mail: s10826325@cycu.edu.tw; s10826329@cycu.edu.tw).

Wei-Yuan Chiang is with the National Synchrotron Radiation Research Center, Hsinchu 30076, Taiwan (e-mail: chiang.wy@nsrrc.org.tw).

Kai-Yi Wong is with the Department of Electrical Engineering, Chung Yuan Christian University, Taoyuan 32023, Taiwan (e-mail: kywong@cycu.edu.tw).

Patricia Angela R. Abu is with the Department of Information Systems and Computer Science, Ateneo de Manila University, Quezon City 1108, Philippines (e-mail: pabu@ateneo.edu).

References

[1] I. K. E. Purnama, I. Kurniastuti, M. Rinastiti, and M. H. Purnomo, "Semi-automatic determination of root canal length in dental X-ray image," in *Proc. 4th Int. Conf. Instrum., Commun., Inf. Technol., Biomed. Eng. (ICICI-BME)*, Nov. 2015, pp. 49–53.

[2] M. U. Ghani and W. C. Karl, "Fast enhanced CT metal artifact reduction using data domain deep learning," *IEEE Trans. Comput. Imag.*, vol. 6, pp. 181–193, 2020.

[3] D. K. Iakovidis, S. V. Georgakopoulos, M. Vasilakakis, A. Koulaouzidis, and V. P. Plagianakos, "Detecting and locating gastrointestinal anomalies using deep learning and iterative cluster unification," *IEEE Trans. Med. Imag.*, vol. 37, no. 10, pp. 2196–2210, Oct. 2018.

[4] G. Ling and C. Cao, "Atomatic detection and diagnosis of severe viral pneumonia CT images based on LDA-SVM," *IEEE Sensors J.*, vol. 20, no. 20, pp. 11927–11934, Oct. 2020.

[5] R. Manzke et al., "Automatic segmentation of rotational X-ray images for anatomic intra-procedural surface generation in atrial fibrillation ablation procedures," *IEEE Trans. Med. Imag.*, vol. 29, no. 2, pp. 260–272, Feb. 2010.

[6] A. Abbas, M. M. Abdelsamea, and M. M. Gaber, "4S-DT: Self-supervised super sample decomposition for transfer learning with application to COVID-19 detection," *IEEE Trans. Neural Netw. Learn. Syst.*, vol. 32, no. 7, pp. 2798–2808, Jul. 2021.

Authorized licensed use limited to: Chung Yuan Christian University. Downloaded on December 15,2022 at 06:18:49 UTC from IEEE Xplore. Restrictions apply.

[7] Y. Zhao et al., "Detecting giant cell tumor of bone lesions using Mueller matrix polarization microscopic imaging and multi-parameters fusion network," *IEEE Sensors J.*, vol. 20, no. 13, pp. 7208–7215, Jul. 2020.

[8] K. Panetta, R. Rajendran, A. Ramesh, S. Rao, and S. Agaian, "Tufts dental database: A multimodal panoramic X-ray dataset for benchmarking diagnostic systems," *IEEE J. Biomed. Health Informat.*, vol. 26, no. 4, pp. 1650–1659, Apr. 2022.

[9] Y.-C. Huang et al., "Tooth position determination by automatic cutting and marking of dental panoramic X-ray film in medical image processing," *Appl. Sci.*, vol. 11, no. 24, p. 11904, Jan. 2021.

[10] F. Umer, S. Habib, and N. Adnan, "Application of deep learning in teeth identification tasks on panoramic radiographs," *Dentomaxillofacial Radiol.*, vol. 51, no. 5, Jul. 2022, Art. no. 20210504.

[11] F. Miao, X. Wang, L. Yin, and Y. Li, "A wearable sensor for arterial stiffness monitoring based on machine learning algorithms," *IEEE Sensors J.*, vol. 19, no. 4, pp. 1426–1434, Feb. 2019.

[12] J. Nayyar, M. Clarke, M. O'Sullivan, and L. F. A. Stassen, "Fractured root tips during dental extractions and retained root fragments. A clinical dilemma?" *Brit. Dental J.*, vol. 218, no. 5, pp. 285–290, Mar. 2015.

[13] A. Hassanzadeh, A. Moulavi, and A. Panahi, "A new capacitive sensor for histomorphometry evaluation of dental implants," *IEEE Sensors J.*, vol. 21, no. 13, pp. 14515–14521, Jul. 2021.

[14] Y.-C. Mao et al., "Caries and restoration detection using bitewing film based on transfer learning with CNNs," *Sensors*, vol. 21, no. 13, p. 4613, Jul. 2021.

[15] S. Patel and M. Goswami, "Comparative analysis of histogram equalization techniques," in *Proc. Int. Conf. Contemp. Comput. Informat. (IC3I)*, Mysore, India, Nov. 2014, pp. 167–168.

[16] Z. Yuan, X. Zhang, P. Zhou, and S. Wang, "Research on indoor position fingerprint location based on machine learning combined particle filter," in *Proc. 2nd Int. Conf. Saf. Produce Informatization (IICSPI)*, Chongqing, China, Nov. 2019, pp. 456–459.

[17] N.-H. Lin et al., "Teeth detection algorithm and teeth condition classification based on convolutional neural networks for dental panoramic radiographs," *J. Med. Imag. Health Informat.*, vol. 8, no. 3, pp. 507–515, Mar. 2018.

[18] S.-Y. Lin and H.-Y. Chang, "Tooth numbering and condition recognition on dental panoramic radiograph images using CNNs," *IEEE Access*, vol. 9, pp. 166008–166026, 2021.

[19] Y. F. Kuo et al., "A convolutional neural network approach for panoramic radiographs classification," *J. Med. Imag. Health Informat.*, vol. 7, pp. 1693–1704, Dec. 2017.

[20] M. P. Muresan, A. R. Barbura, and S. Nedevschi, "Teeth detection and dental problem classification in panoramic X-ray images using deep learning and image processing techniques," in *Proc. IEEE 16th Int. Conf. Intell. Comput. Commun. Process. (ICCP)*, Sep. 2020, pp. 457–463.

[21] S. Hou, Y. Chu, and J. Fei, "Robust intelligent control for a class of power-electronic converters using neuro-fuzzy learning mechanism," *IEEE Trans. Power Electron.*, vol. 36, no. 8, pp. 9441–9452, Aug. 2021.

[22] M. Usman, A. Carie, B. Marapelli, H. D. Bedru, and K. Biswas, "A human-in-the-loop probabilistic CNN-fuzzy logic framework for accident prediction in vehicular networks," *IEEE Sensors J.*, vol. 21, no. 14, pp. 15496–15503, Jul. 2021.

[23] S.-L. Chen et al., "Dental shade matching method based on hue, saturation, value color model with machine learning and fuzzy decision," *Sensors Mater.*, vol. 32, no. 10, pp. 1–15, Oct. 2020.

[24] C.-W. Li et al., "Detection of dental apical lesions using CNNs on periapical radiograph," *Sensors*, vol. 21, no. 21, p. 7049, Oct. 2021.

[25] C. A. Gutierrez and M. Patzold, "The Riemann sum method for the design of sum-of-cisoids simulators for Rayleigh fading channels in non-isotropic scattering environments," in *Proc. Int. Conf. Ultra Modern Telecommun. Workshops*, Oct. 2009, pp. 1–5.

[26] X. Bai and F. Zhou, "Unified form for multi-scale top-hat transform based algorithms," in *Proc. 3rd Int. Congr. Image Signal Process.*, Oct. 2010, pp. 1097–1100.

[27] S.-L. Chen and H.-J. Tsai, "A novel adaptive local dimming backlight control chip design based on Gaussian distribution for liquid crystal displays," *IEEE J. Display Technol.*, vol. 12, no. 12, pp. 1494–1505, Dec. 2016.

[28] S.-J. Ko, A. Morales, and K.-H. Lee, "Block basis matrix implementation of the morphological open-closing and close-opening," *IEEE Signal Process. Lett.*, vol. 2, no. 1, pp. 7–9, Jan. 1995.



Shih-Lun Chen (Member, IEEE) received the B.S., M.S., and Ph.D. degrees in electrical engineering from National Cheng Kung University, Tainan, Taiwan, in 2002, 2004, and 2011, respectively.

He was an Assistant Professor with the Department of Electronic Engineering and an Associate Professor with the Department of Electronic Engineering, Chung Yuan Christian University, Taoyuan, Taiwan, from 2011 to 2014 and 2014 to 2017, respectively, where he has been a Professor with the Department of Electronic Engineering since 2017. His current research interests include VLSI chip design, image processing, wireless body sensor networks, the Internet of Things, wearable devices, data compression, fuzzy logic control, biomedical signal processing, and reconfigurable architecture.

Dr. Chen was a recipient of the Outstanding Teaching Awards from Chung Yuan Christian University in 2014 and 2019, respectively.



Tsung-Yi Chen received the B.S. degree in electronic engineering from Chung Yuan Christian University, Taoyuan, Taiwan, in 2020, where he is currently pursuing the Ph.D. degree.

His current research interests include VLSI chip design, image processing, machine learning, and biomedical signal processing.



Yi-Cheng Mao was born in Taipei, Taiwan, in 1990. He received the bachelor's degree in dentistry from Chung Shan Medical University, Taichung, Taiwan, in 2015.

He was a resident who is having operative dentistry specialist training at the Department of General Dentistry, Chang Gang Memorial Hospital, Taoyuan, Taiwan, since 2016, and received his Operative Dentistry Specialist Certificate from the Taiwan Academy of Operative Dentistry in 2020. He has been an Attending Doctor of General Dentistry with the Chang Gang Memorial Hospital since 2021.



Szu-Yin Lin (Member, IEEE) received the Ph.D. degree from National Chiao Tung University, Hsinchu, Taiwan, in 2012.

He is currently a Professor with the Department of Computer Science and Information Engineering, National Ilan University (NIU), Yilan, Taiwan. His research interests include the areas of intelligent data analysis, artificial intelligence, machine learning, deep learning, management information systems, and service-oriented computing.

Authorized licensed use limited to: Chung Yuan Christian University. Downloaded on December 15,2022 at 06:18:49 UTC from IEEE Xplore. Restrictions apply.



Ya-Yun Huang received the B.S. degree in electronic engineering from Chung Yuan Christian University, Taoyuan, Taiwan, in 2021, where she is currently pursuing the master's degree.

Her current research interests include VLSI chip design, image processing, and image compression.



Chiung-An Chen received the B.S. degree in electronic engineering from Chung Yuan Christian University, Taoyuan, Taiwan, in 2005, and the Ph.D. degree in electrical engineering from National Cheng Kung University, Tainan, Taiwan, in 2013.

Since 2017, she has been an Assistant Professor with the Department of Electrical Engineering, Ming Chi University of Technology, Taipei, Taiwan. Her current research interests include VLSI chip design, image processing, and wireless body sensor networks, the Internet of Things, wearable devices, biomedical signals, and image processing.



Yuan-Jin Lin has been studying electronic engineering and computer science at Chung Yuan Christian University, Taoyuan, Taiwan, since 2022.

His current research interests include VLSI chip design, image processing, and machine learning.



Yo-Ming Hsu is currently pursuing the B.S. degree in electrical engineering and computer science with Chung Yuan Christian University, Taoyuan, Taiwan.

His current research focuses on image processing, machine learning, and field programmable gate array (FPGA) programming.



Chi-An Li received the B.S. degree in electronic engineering from Chung Yuan Christian University, Taoyuan, Taiwan, in 2020, where she is currently pursuing the master's degree.

Her current research interests include VLSI chip design, image processing, and biomedical signal processing.



Wei-Yuan Chiang received the B.S. degree in physics from Chung Yuan Christian University, Taoyuan, Taiwan, in 2001, and the M.S. and Ph.D. degrees in physics from National Tsing Hua University, Hsinchu, Taiwan, in 2003 and 2008, respectively.

He was an Assistant Professor with the Department of Electrical Engineering, Ming Chi University of Technology, Taipei, Taiwan, from 2015 to 2020. He has been an Assistant Engineer with the Light Source Division, National Synchrotron Radiation Research Center, Hsinchu, since 2021. His current research interests include electromagnetism, microwave source, microwave processing of advanced materials, microwave physics, and engineering.



Kai-Yi Wong received the B.S. and M.S. degrees from the Department of Electrical and Computer Engineering, Tamkang University (TKU), New Taipei City, Taiwan, in 2015 and 2017, respectively, and the Ph.D. degree from the Department of Mechanical and Intelligent Systems Engineering, The University of Electro-Communications (UEC), Tokyo, Japan, in 2021.

She is currently an Assistant Professor with the Department of Electrical Engineering, Chung Yuan Christian University (CYCU), Taoyuan, Taiwan. Her research interests include robotics, intelligent systems, machine learning, and nonlinear systems control.



Patricia Angela R. Abu (Member, IEEE) received the B.S. degree in electronics and communications engineering and the the M.S. degree in electronics engineering with a major in microelectronics from Chung Yuan Christian University, Taoyuan, Taiwan, in 2007 and 2009, respectively, and the Ph.D. degree in computer science from the Ateneo de Manila University, Quezon City, Philippines, in 2015.

She is the Research Lab Head of the Ateneo Laboratory for Intelligent Visual Environments (ALIVE) and an Assistant Professor with the Department of Information Systems and Computer Science (DISCS), Ateneo de Manila University. Her current research focuses on image processing and computer vision with applications that revolve on biomedical imaging and road/transportation, anomaly detection, and the Internet of Things (IoT) systems that granted ALIVE several best research paper and presentation awards both local and abroad.

Authorized licensed use limited to: Chung Yuan Christian University. Downloaded on December 15,2022 at 06:18:49 UTC from IEEE Xplore. Restrictions apply.